Design of Calibrators for Extruded Profiles. Part I: Modeling the Thermal Interchanges

J. M. NÓBREGA[1], O. S. CARNEIRO[1]*, J. A. COVAS[1], F. T. PINHO[2], *and* P. J. OLIVEIRA[3]

[1]*IPC–Institute for Polymers and Composites*
Department of Polymer Engineering
University of Minho
4800-058 Guimarães, Portugal

[2]*Centro de Estudos de Fenómenos de Transporte*
DEMEGI
Faculdade de Engenharia da Universidade do Porto
Rua Dr. Roberto Frias, 4200-465 Porto, Portugal

[3]*Departamento de Engenharia Electromecânica*
Universidade da Beira Interior
Rua Marquês D'Ávila e Bolama, 6201-001 Covilhã, Portugal

The parameters influencing the calibration/cooling stage of profile extrusion are discussed, and a numerical finite-volume method code to model the heat transfer is described and validated. For this purpose, the numerical predictions are compared with the analytical solution of a simple problem, with results available in the literature and with those produced by a commercial software. The routines developed are then used to identify the main process parameters and boundary conditions and to estimate their relative importance. The investigation clearly shows the advantages of using several calibrators separated by annealing zones, relative to a single calibrator of the same total length, and the large impact of the contact resistance between extrudate and cooling unit while showing negligible impact of other boundary conditions. A decrease of the extrudate velocity is seen to be also an effective control parameter, but it decreases the production rates. Polym. Eng. Sci. 44:2216–2228, 2004.

INTRODUCTION

As shown in *Fig. 1*, a typical plastics extrusion line for the production of profiles comprises an extruder, a die, a calibration/cooling table (which can include several units), a haul-off and a saw (or, alternatively, a coiling device). The viscoelastic nature of the polymer melt, together with unavoidable fluctuations of the operating conditions (which affect the rheological behavior and flow dynamics), makes it very difficult to produce an extrudate with the required cross section. Moreover, as the profile progresses along the production line, it is subjected to a variety of external forces (such as friction, gravity, buoyancy and compression), which can cause important deformations, unless efficient cooling ensures enough profile strength (1, 2). Therefore, the calibration/cooling step has a double objective: it prescribes the final dimensions of the profile, while cooling it fast to solidify the outer layers of the extrudate to ensure sufficient rigidity during the remainder cooling steps (1). This is seen in *Fig. 1*, after the first calibrator, where a layer with thickness δ has been cooled to a temperature below the solidification temperature (T_s). After calibration, the average profile temperature should also be lower than T_s to avoid subsequent remelting (1). Cooling of the extrudate should be as uniform as possible, meaning that the temperature gradients along the profile contour and thickness should be minimized, in order to induce adequate morphology development and a reduced level of residual thermal stresses (3, 4). Therefore, the objective is to

*To whom correspondence should be addressed. E-mail: olgasc@dep.uminho.pt

Published online in Wiley InterScience (www.interscience.wiley.com).
DOI: 10.1002/pen.20249

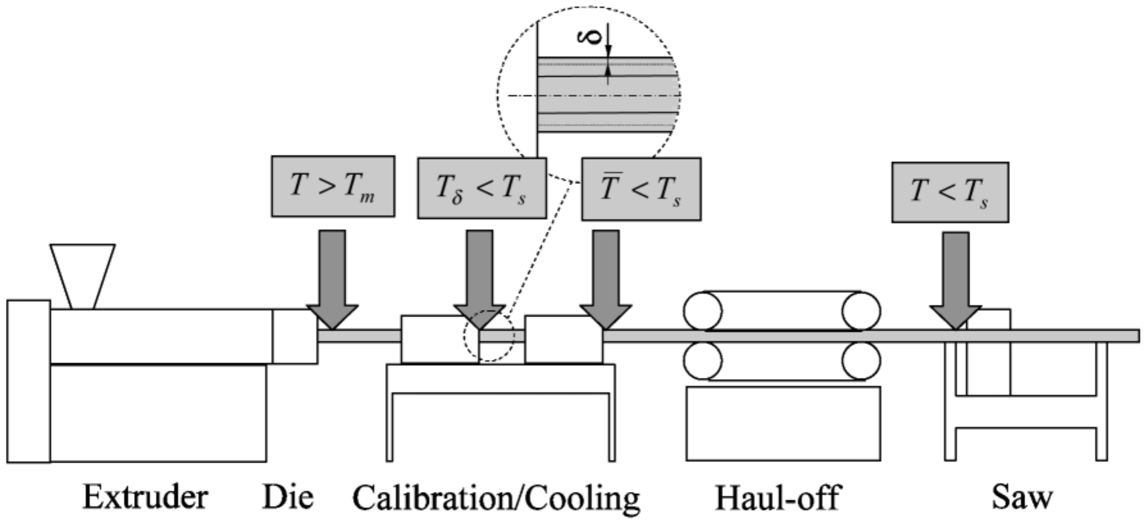

Fig. 1. Typical extrusion line for the production of thermoplastic profiles (adapted from (1)).

minimize both the profile average temperature and the corresponding temperature nonhomogenity.

The calibration can be carried out by applying either internal pressure or external vacuum. It can also be wet and/or dry, i.e., either direct or indirect contact takes place between the cooling medium (generally, water) and the hot profile, respectively (5, 6). Usually, several calibrators are used in series, separated by relatively short air zones (7, 8), where the temperature tends to equalize, to minimize the internal thermal induced stresses and increase the heat transfer efficiency in the next calibrator. For high-speed profile extrusion, vacuum-assisted dry calibration has proved to be particularly reliable (5). Sometimes, a combined wet/dry system is used, consisting of a dry vacuum block unit followed by a series of water-cooling blocks.

Given the above, the parameters that influence the thermal performance of the calibration system may be grouped as follows:

i) *system geometry*—number of calibrating units, unit length, separating distance and layout of the cooling channels (the latter involves such quantities as number, diameter, type of arrangement, distance between consecutive channels and distance to the profile) (6, 9);

ii) *cooling conditions*—temperature of the inlet water, flow rate, flow direction and wet versus dry contact with the profile (1, 2);

iii) *vacuum conditions*—number and location of vacuum holes and vacuum pressure;

iv) *extrusion conditions*—mass flow rate and cross-temperature profile field at die exit;

v) *polymer thermo*—physical properties-thermal diffusivity and thermal expansion coefficient;

vi) *properties of the calibrator material*—thermal conductivity and surface roughness;

vii) *profile cross section*—thicknesses, number and location of hollow sections, etc.

Despite their obvious practical relevance, calibrating and cooling systems have attracted relatively little attention in the scientific literature. Most available reports concern the calculation of the time evolution of the extrudate temperature (8–10), the exception being the work of Fradette *et al.* (3), in which the model previously developed (9) was integrated in an optimization routine used to determine the optimal location and size of the cooling channels. However, a thorough study of the influence of the above geometrical, material, process and operational parameters on the cooling performance is apparently not available. In fact, the existing results are either qualitative or concentrate on a few variables (10, 11), ignoring, for instance, the effect of boundary conditions. Moreover, no methodology for the design of calibrators has yet been proposed.

The authors aim to develop and validate an algorithm for the thermal design of calibrators for thermoplastic extrudates. As for other plastics-processing equipment, an optimization approach seems well suited for this purpose (12, 13). It should comprise an objective function quantifying the calibrator performance, an optimization algorithm assessing and generating increasingly more efficient solutions, and a modeling package describing the process response. For this purpose, this work presents and validates a 3D code based on the finite-volume method (FVM) to model the thermal interchanges during the calibration and cooling stage of profile extrusion. FVM software is faster and requires less computational resources than its FEM counterpart (14), which is essential for the recurring use required by the optimization algorithm. With a view to design, a study of the influence of the boundary conditions, geometrical and operating parameters on the performance of cooling is also carried out. The actual design methodology will be discussed in a forthcoming paper.

PROCESS MODELING

The first attempts to model the cooling of plastic profiles or pipes were made during the 1970s and 1980s with 1D models (see, for example (7, 15, 16)), which were applicable only to idealized conditions, such as uniform cooling and uniform thickness extrudates. Menges *et al.* (17) developed a 2D FEM approach that could deal with any extrudate cross section, but ignored axial heat fluxes. Inclusion of axial diffusion was addressed by Sheehy *et al.* (9), who proposed the Corrected Slice Model (CMS), which is a hybrid 2D model that can cope with the three-dimensionality introduced by the axial heat fluxes. Other 2D modeling studies of extrudate cooling addressed other specific aspects, such as the inclusion of more realistic boundary conditions for the heat exchange within the internal cavities of hollow profiles (11, 18), or the prediction of sag flow in thick wall pipes (19).

A major difficulty facing the modeling of the cooling process is the adequate knowledge of the heat transfer coefficient, h, between the profile surface and the cooling medium, i.e., calibrator internal walls, water or air, which must include the effect of the contact resistance. It was experimentally shown that h can vary significantly (20), depending on the location along the calibration system. Other authors estimate h empirically, considering the local effectiveness of the contact between the profile and the calibrator from observations of the wear pattern of the calibrator (10). Finally, values of h can also be estimated using an inverse problem strategy, i.e., determining the values of the coefficient that match numerical simulations with the corresponding experimental temperature fields (8, 21). *Table 1* summarizes the values of h reported in the literature for calibration/cooling systems.

Outline of the Numerical Procedure

In this work, the thermal field in the calibrating and cooling system is calculated by a 3D computational code based on the finite-volume method. This code was initially developed for the computation of isothermal viscoelastic flows, and has been recently extended to the case of non-isothermal flows (22). The details of the numerical algorithm and of its implementation have been described elsewhere (23, 24). The code is used to numerically calculate the variation of the temperature field within the extrudate as well as within the calibrator. Therefore, the energy conservation equations to be solved here can be written as

$$\frac{\partial}{\partial x}\left(k_p \frac{\partial T_p}{\partial x}\right) + \frac{\partial}{\partial y}\left(k_p \frac{\partial T_p}{\partial y}\right) + \frac{\partial}{\partial z}\left(k_p \frac{\partial T_p}{\partial z}\right) - \frac{\partial}{\partial z}\left(\rho_p c_p w T_p\right) = 0 \qquad (1)$$

for the profile, and as

Table 1. Values Reported for the Heat Transfer Coefficient (h).

Geometry	Situation	h [W/m^{2}K]	Determination/Reference
Profile	Polymer/calibrator (dry)	200	Empirical evaluation (10)
	Polymer/calibrator (wet)	500	
	Polymer/calibrator (air gap)	50	
	Polymer/calibrator (poor contact)	Reduction of 2/3 of thecorresponding good contact	
	Polymer/air free convection (inner cavities)	10	
	Polymer/water (good circulation)	250	
	Polymer/water (poor circulation)	100	
	Polymer/calibrator	1000	(9)
	Polymer/calibrator (along the calibrator axis)	h = exp (9.2 − 1.3F_0), with $F_0 = (\alpha t)/\delta^2$ α−thermal diffusivity t−cooling time δ−profile thickness	Matching of numerical simulations with experimental results (20)
	Annealing zones	5	
Pipe (∅ 63−315 mm)	1st Vacuum tank (spray cooling)	700−2000	Matching of numerical simulations with experimental results (8, 21)
	2nd Vacuum tank (spray cooling)	170−750	
	3rd Vacuum tank (spray cooling)	120−550	
	Annealing zones	14−35	

$$\frac{\partial}{\partial x}\left(k_c\frac{\partial T_c}{\partial x}\right)+\frac{\partial}{\partial y}\left(k_c\frac{\partial T_c}{\partial y}\right)+\frac{\partial}{\partial z}\left(k_c\frac{\partial Tc}{\partial z}\right)=0 \quad (2)$$

for the calibrator, where T is the medium temperature, w is the longitudinal velocity component (extrusion direction) in a Cartesian coordinate frame, ρ is the fluid density, k is the thermal conductivity and c is the specific heat. The subscripts p and c denote polymer and calibrator, respectively.

In order to account for real processing conditions, various temperature and heat flux boundary conditions were implemented. At the interface between the profile and the calibrator, either perfect contact, assuming both temperature and heat flux continuity,

$$(T_p = T_c)_{\text{interface}} \quad (3)$$

$$k_c\left(\frac{\partial T_c}{\partial n}\right)_{\text{interface}} = -k_p\left(\frac{\partial T_p}{\partial n}\right)_{\text{interface}} \quad (4)$$

or the existence of a temperature discontinuity (i.e., a thermal contact resistance (20))

$$k_c\left(\frac{\partial T_c}{\partial n}\right)_{\text{interface}} = -k_p\left(\frac{\partial T_p}{\partial n}\right)_{\text{interface}} = h_i(T_p - T_c)_{\text{interface}} \quad (5)$$

was considered. Here, h_i is the interface heat transfer coefficient and n is the normal vector of the interface. At the interface between the outside walls of the calibrator and the surrounding air, or between the external extrudate surface and the surrounding air, adiabatic or natural convection and radiation boundary conditions were set up. *Figure 2* summarizes the boundary conditions considered in a typical problem.

Equations 1 and *2* are discretized following a finite-volume approach, and the resulting sets of linear algebraic equations are solved iteratively and sequentially, assuming an imposed heat flux at the polymer/calibrator interface. The coupling between the temperature fields in the polymer and calibrator domains is dealt with as follows. At each iteration step, the interface temperatures obtained for both domains are used to update the interface heat flux values (which depend on the type of boundary condition assumed at the interface), by using either *Eq 4* or *Eq 5*, and the whole procedure is repeated until the temperature field converges.

Geometry and Mesh Generators

Given that the numerical procedure outlined above will be used intensively for design purposes, where it is necessary to evaluate the performance of various tentative calibrator designs (this will be dealt with in a future publication), specialized routines were developed to generate automatically the geometrical layout of the calibrator and the corresponding mesh.

The former requires information on the profile cross section, number of calibrators and, for each calibrator, the corresponding dimensions, location, number and layout of the cooling channels (these can be machined longitudinally, transversally or in a zigzag arrangement). When the mesh is generated, the presence of the cooling channels is initially ignored. Subsequently, the cells corresponding to the latter are removed and the adequate boundary conditions are imposed to their neighbor cell faces. This approach generates a stepwise approximation of the geometry of the cooling channels (25), akin to the "virtual boundary conditions" employed by Sheehy *et al.* (9) for the same purpose. *Figure 3* depicts an example of an automatically generated mesh corresponding to the geometry shown in *Fig. 2*.

The finite-volume routine requires information on the computational mesh (x, y, and z coordinates of all mesh points) and connectivity arrays to allow the identification of all control volumes surrounding a given computational cell. With this information, it is possible to evaluate cell face areas, cell volumes and distances that are needed for the discretization of the governing differential equations.

MODEL ASSESSMENT

Direct confrontation between predictions and experimental data is difficult, since the practical measurement

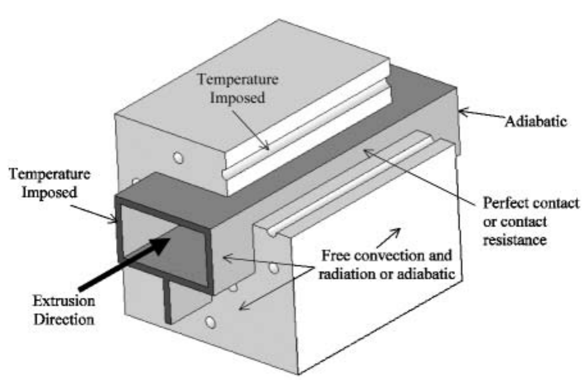

Fig. 2. Thermal boundary conditions considered.

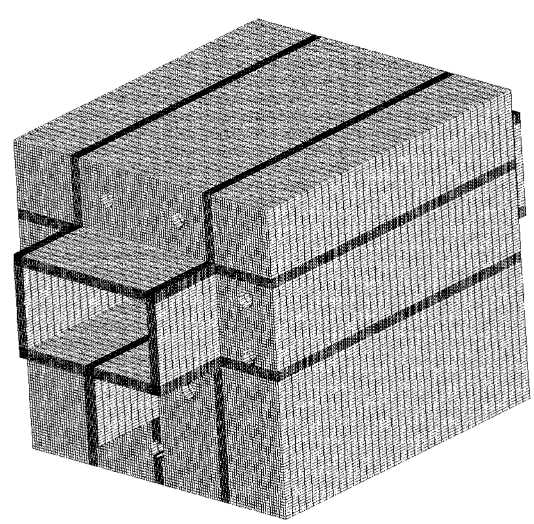

Fig. 3. Mesh corresponding to the geometry shown in Fig. 2.

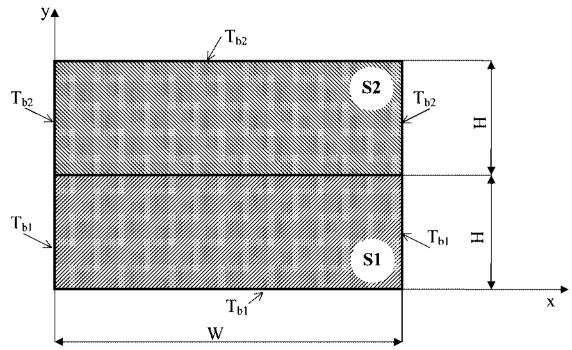

Fig. 4. Geometry and boundary conditions for the 'Analytical' problem.

of the temperature profiles within and along the extrudate cross section, especially when the extrudate moves along the calibration/cooling system, is extremely difficult, requiring the use of thermocouples imbedded in the material, at different depths of the profile thickness, and moving with the profile (8). Profile surface temperatures between two consecutive calibrators are easier to monitor, but the quality of the measurements depends on the emissivity settings used in the noncontact infrared thermometers that are generally employed and also on the measuring depth, i.e., the thickness effectively reached by the radiation from the sensor (26). However, most of the temperature measurements reported concern pipes (1, 8, 19, 21, 27) rather than profiles (20), and, even in this case, the data presented are insufficient for modeling purposes.

Therefore, the model developed and presented in this work is assessed by comparing its predictions with: i) the analytical results derived for a simple geometry, ii) the results reported by Sheehy *et al.* (9) for a more complex layout, and iii) the calculations provided by a general purpose FEM software (Polyflow (28)).

Analytical Solution

The first case study considered is illustrated in *Fig. 4*. It consists of two rectangular slabs, S1 and S2, with thermal conductivities k_1 and k_2, respectively, in contact through one of their faces. As shown also in the figure, the temperature is imposed on the remaining faces. The energy equation (2) controlling the temperature distribution on each slab, for constant conductivity, takes the form:

$$\frac{\partial^2 T}{\partial x^2} + \frac{\partial^2 T}{\partial y^2} = 0 \tag{6}$$

As described by Nóbrega (29), the temperature distribution in each slab can be obtained from:

$$T = T_{b1} + \sum_{n=1}^{\infty} \frac{2}{\pi}(T_{b2} - T_{b1}) \frac{(-1)^{n+1}+1}{n} \frac{-k_2}{(k_2+k_1)} \sin\left(\frac{n\pi x}{W}\right) \sinh\left(\frac{n\pi y}{W}\right) \tag{7}$$

for S1, and from

$$T = T_{b2} + \sum_{n=1}^{\infty} \frac{2}{\pi}(T_{b2} - T_{b1}) \frac{(-1)^{n+1}+1}{n} \frac{k_1}{(k_2+k_1)} \sin\left(\frac{n\pi x}{W}\right) \sinh\left(\frac{n\pi(-y+2H)}{W}\right) \tag{8}$$

for S2, for perfect contact case, and by:

$$T = T_{b1} + \sum_{n=1}^{\infty}\left[\frac{2}{\pi} h_i (T_{b1} - T_{b2}) \frac{(-1)^{n+1}+1}{n} \frac{1}{-k_1\frac{n\pi}{W}\cosh\left(\frac{n\pi H}{W}\right) - \left(\frac{k_2+k_1}{k_2}\right)\sinh\left(\frac{n\pi H}{W}\right)} \sin\left(\frac{n\pi x}{W}\right)\sinh\left(\frac{n\pi y}{W}\right)\right] \tag{9}$$

for S1 and from

$$T = T_{b1} + \sum_{n=1}^{\infty}\left[\frac{2}{\pi} h_i (T_{b1} - T_{b2}) \frac{(-1)^{n+1}+1}{n} \frac{1}{k_2\frac{n\pi}{W}\cosh\left(\frac{n\pi H}{W}\right) + \left(\frac{k_2+k_1}{k_1}\right)\sinh\left(\frac{n\pi H}{W}\right)} \sin\left(\frac{n\pi x}{W}\right)\sinh\left(\frac{n\pi(-y+2H)}{W}\right)\right] \tag{10}$$

for S2, when the interface is modeled with a contact resistance boundary condition.

The temperature distributions defined by *Eqs 7–10*, both for perfect contact or thermal resistance, are compared in *Fig. 5* with those obtained in the developed numerical routine, using $W = 100$ mm, $H = 50$ mm, $T_{b1} = 100°C$, $T_{b2} = 180°C$, $k_1 = 7$ W/mK, $k_2 = 14$ W/mK and, for the case of contact resistance, $h_i = 500$ W/m^{2}K. It is clear that the two sets of results are virtually coincident, hence giving confidence on the correct implementation of the thermal routines.

Complex Layouts

The predictions of the numerical routines developed were also compared with the results of Sheehy *et al.* (9) for the problem shown in *Fig. 6*, which was used by those authors to validate the Corrected Slice Model (CSM). The problem consists of the determination of the temperature distribution in a 2-mm-thick polymeric sheet moving at 0.01 m/s while being cooled by a 50-mm-long and 10-mm-thick calibrator containing three transverse cooling channels. The thermal and physical properties of the calibrator (subscript c) and polymer (subscript p) are: $k_p = 0.18$ W/mK, $k_c = 23.0$ W/mK, $\rho_p = 1400$ kg/m^3 and $c_p = 1000$ J/kgK. The thermal boundary conditions are also identified in *Fig. 6*. According to Sheehy *et al.* (9), the rigorous thermal solution of the problem is that shown in *Fig. 7a*. It is seen that the isotherms close to the calibrator inlet are perpendicular to the interface, indicating that there is no

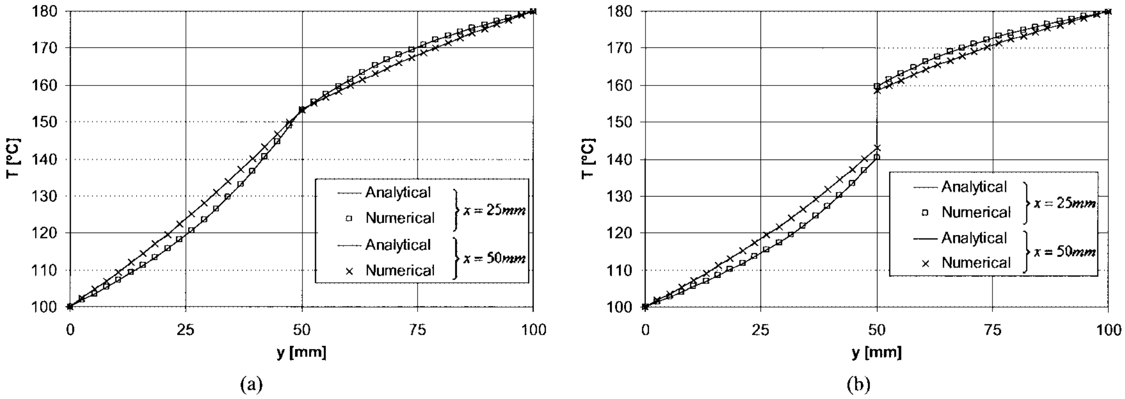

Fig. 5. Analytical and numerical results for the temperature distribution of the 'Analytical' problem: (a) perfect contact; (b) contact resistance.

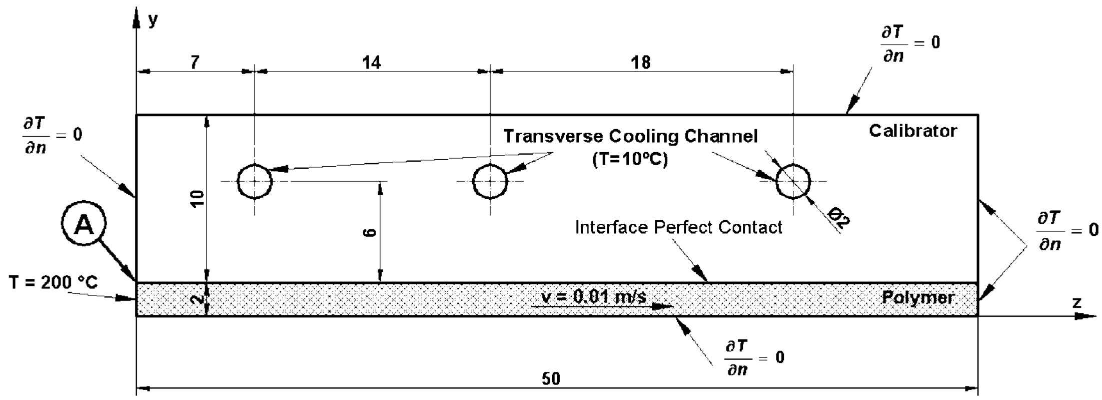

Fig. 6. Description of the 'Complex Layout' problem (dimensions in mm).

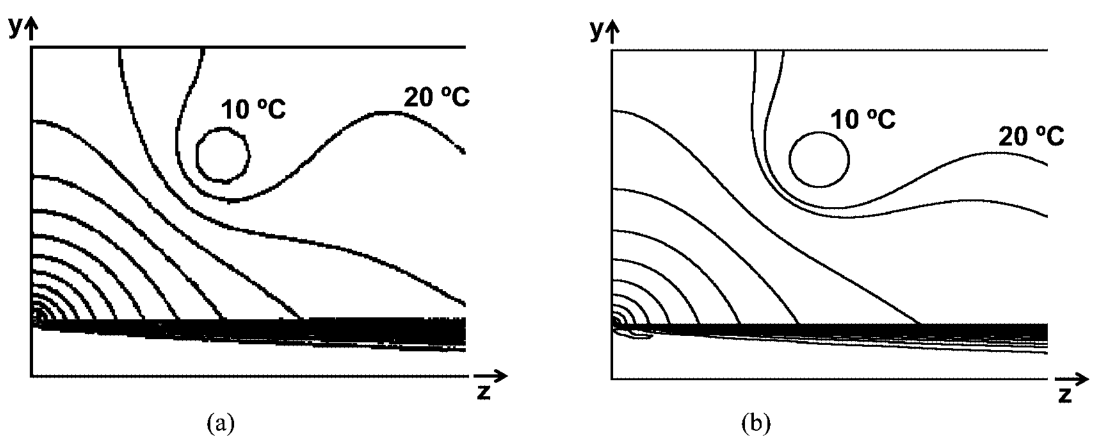

Fig. 7. Temperature distribution for the 'Complex Layout' problem: (a) solution considered as rigorous by Sheehy et al. (9); (b) same as a), calculated by Polyflow.

heat exchange across the interface, i.e., the temperature gradient in direction normal to the interface looks to be zero, a physically unrealistic scenario. This is a consequence of assuming that the temperature of the calibrator at the corner next to the extrudate (point A in *Fig. 6*) is equal to the melt inlet temperature. Given the higher conductivity of the calibrator, the inlet melt temperature would spread out easily to the corner neighborhood, and, under these conditions, no heat exchange would occur between the calibrator and the profile. It is probable that the high temperature imposed at the calibrator corner was set because both domains (calibrator and polymer) share the same node. This hypothesis was confirmed with Polyflow: its results, shown in *Fig. 7b*, are very similar to those of *Fig. 7a*, and were obtained considering a single node at point A with an imposed temperature of 200°C.

Given the above discussion, the problem studied by Sheehy *et al.* (9) was slightly modified here. Now, the polymer domain, where the temperature is imposed, begins 1 mm ahead of the calibrator entrance, as represented in *Fig. 8*. The new temperature distribution determined by Polyflow (see *Fig. 9a*) shows, as expected, heat exchange between the polymer and the beginning of the calibrator.

A more realistic modeling of the original problem of Sheehy *et al.* (9) requires the use of a coincident double-node technique, one belonging to the polymer and the other to the calibrator, to allow for a temperature discontinuity between the two domains. The results of the calculations with our code are shown in *Fig. 9b*, using the double-node technique, and should be contrasted directly with those of Polyflow in *Fig. 9a*. A good agreement is observed between both solutions, and this is further confirmed in *Fig. 10*, which compares temperature profiles across the sheet at three different axial locations (z/L = 7/50, 30/50 and 50/50, where L is the length of the calibrator).

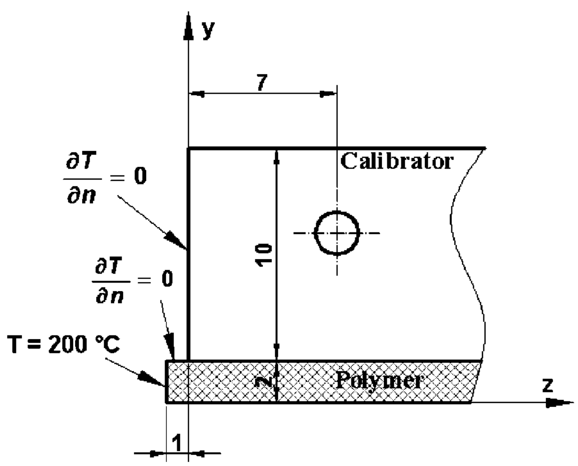

Fig. 8. Modified 'Complex Layout' problem (dimensions in mm).

It is worth mentioning that despite the problems discussed above, the results of Sheehy *et al.* (9) using the CSM are reasonably accurate: the average polymer outlet temperature was predicted as 122.3°C, with the model referred to as rigorous by those authors, and 120.3°C, with the CSM; we obtained 120.6°C.

Finally, the numerical code developed in this work was also assessed for the third test case study illustrated in *Fig. 11*, representing the behavior of the polymer sheet downstream from the calibration, in the annealing zone that further exposes the extrudate to cold air and homogenizes the polymer temperature distribution, as a consequence of heat fluxes from hotter to cooler regions. This situation is quite relevant for the study of systems having more than one cooling/calibrating unit (see *Fig. 12b*). The temperature distribution at the end of the annealing zone, shown in *Fig. 10*, corresponds to z/L = 75/50. The predictions of our finite-volume code and those of Polyflow are compared, and again, the agreement is excellent.

INFLUENCE OF BOUNDARY CONDITIONS, PROCESS, AND GEOMETRICAL PARAMETERS

Next, the code is used to investigate the effect of some boundary conditions, process, and geometrical parameters on the behavior and performance of calibrating/cooling systems. For this purpose the cooling of the rectangular hollow profile shown in *Fig. 12* was studied under the general conditions summarized in *Table 2*. A calibration length of 600 mm was fixed but it corresponded to either a single or three consecutive calibration units. The results obtained with the various systems were compared in terms of heat fluxes at the geometry boundaries and of minimum (T_{min}), maximum (T_{max}) and average ($\bar{T}$) temperatures and the temperature distribution standard deviation (σ_T) calculated at

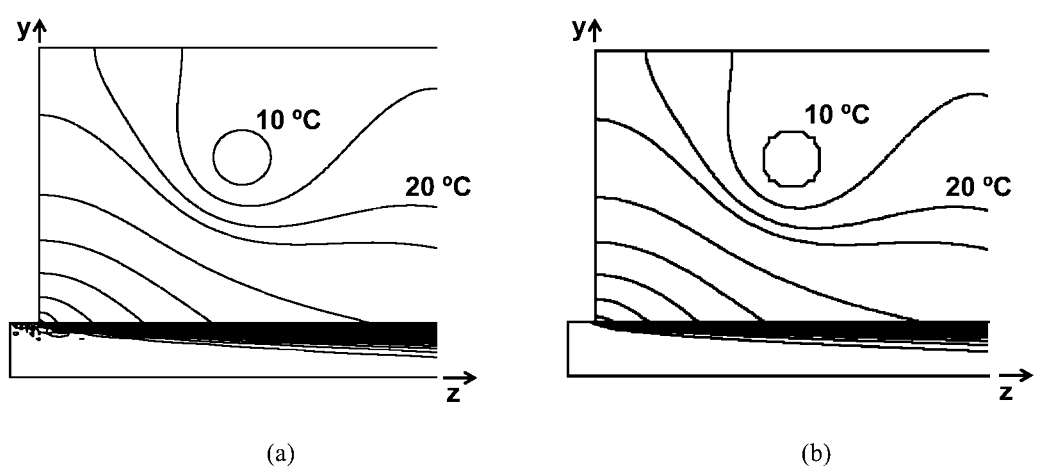

Fig. 9. Temperature distribution for the modified 'Complex Layout' problem: (a) solution calculated by Polyflow; (b) same as a), calculated with the numerical routine developed in this work.

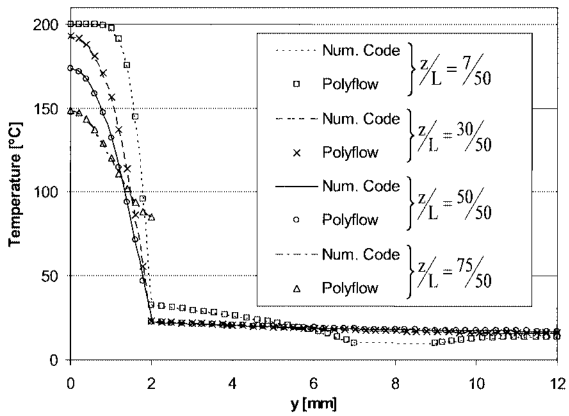

Fig. 10. Temperature distributions for 'Complex Layout' problems of Fig. 6 (z/L = 7/50; z/L = 30/50; z/L = 50/50) and described in Fig. 8 (z/L = 75/50).

the end cross section of the polymer extrudate. The latter is computed as:

$$\sigma_T = \frac{\sum_{i=1}^{n_f} (T_i - \bar{T})^2 A_i}{A_T} \tag{11}$$

where n_f is the number of computational cell faces on the profile outlet boundary, T_i is the face temperature, A_i is the face area and A_T is the area of the profile cross section. Therefore, σ_T is a measure of the temperature nonhomogeneity at the final cross section.

It is worth mentioning that the results obtained for this profile geometry under study cannot be directly extrapolated to other geometries, but, nevertheless, the results provide information on the qualitative effect of the main variables involved in the process and their relative importance.

Boundary Conditions

An important issue for modeling the profile cooling stage is the definition of the boundary conditions at the profile and calibrator surfaces. In the literature, the outer surfaces of both profile and calibrator are modeled either as adiabatic (9) or having a defined convective heat flux (8), in both cases neglecting radiation. For the interface between the profile and the calibrator, either perfect contact or contact resistance is used; some authors argue that contact resistance is the better choice (1), but in reality we are unaware of any practical or computational quantification of its relevance. Thus, in order to study the influence of this parameter, cooling of the profile presented in *Fig. 12a* was modeled, adopting the layout shown in *Fig. 12b*, where the cooling length of 600 mm was divided into three 200-mm-long calibrators, separated by 75-mm-long annealing zones. In this figure, Os1 to Os4 represents the profile outer surfaces, i.e., exposed to the surrounding environment along the cooling line. The set of case studies considered is described in *Table 3*, while the computed results are summarized in *Tables 4* and *5*.

Table 4 compares the heat fluxes at the various boundaries. Starting with the reference case study *c1r1*, which accounts both convection and radiation at the outer boundaries, the table shows losses of 32.0, 20.7, 15.0 and 7.5 W through the extrudate outer surfaces Os1 through Os4, respectively, and losses of 1076.1, 736.3 and 589.8 in the three calibrators mostly via the cooling channels. *Table 5* contains data for temperature at the cross section at the end of the extrudate. As shown in *Table 4*, most of the heat is removed from the profile through its interface with the calibrator, and then from the calibrator through the cooling channels. Consequently, the values in *Table 5* are little affected by the type of boundary condition considered at the extrudate and calibrator outer surfaces, and, in contrast, the conditions at the interface between the extrudate and the calibrator are fundamental as can be seen in the total loss. In fact, changes in the resistance coefficient (h_i) have the highest impact on the total heat loss (compare $h\uparrow$, $h\downarrow$ and pc with the reference case). The effects of radiation and convective heat transfer are similar, but since most of the cooling takes place via the

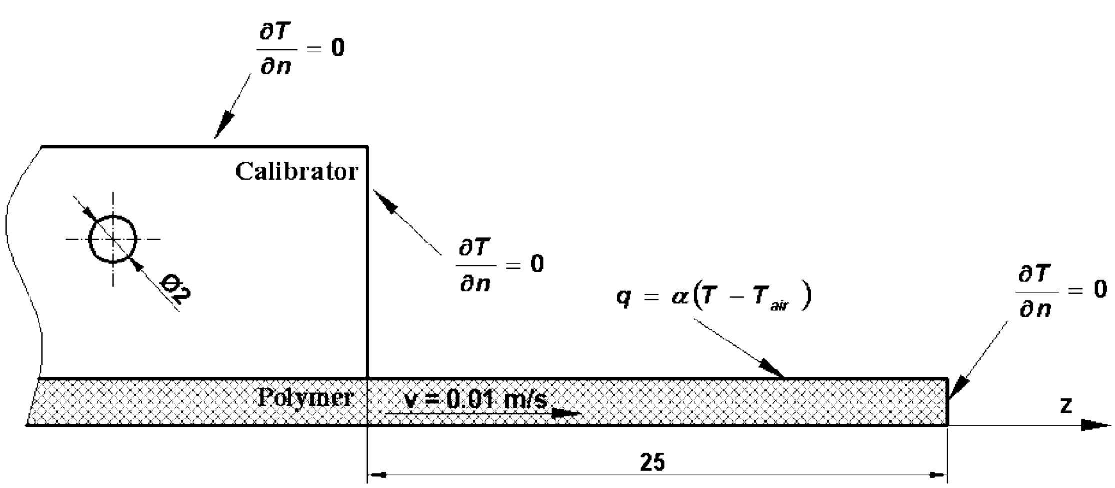

Fig. 11. Modified 'Complex Layout' problem considering an annealing zone downstream (dimensions in mm).

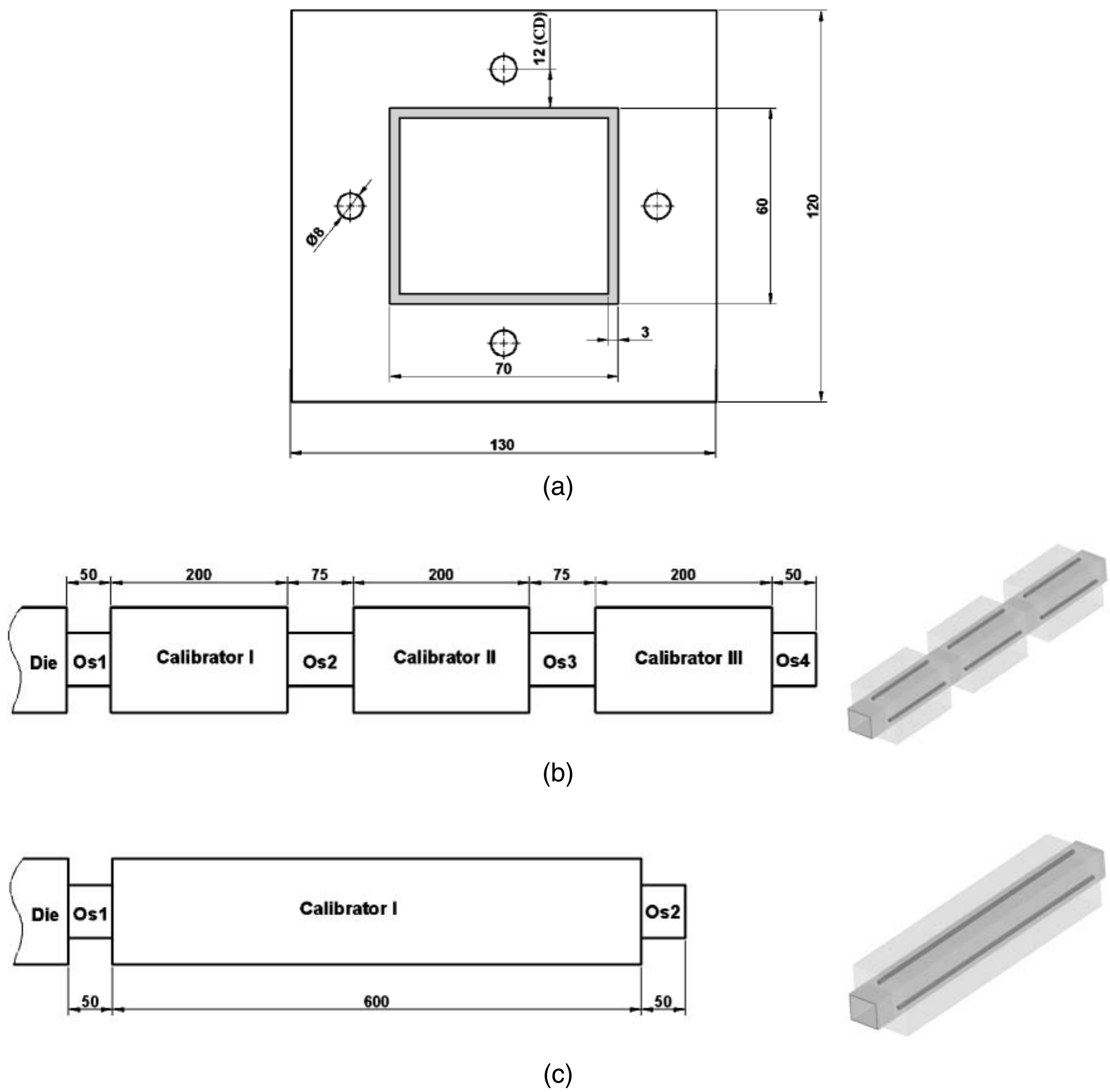

Fig. 12. Cooling of a rectangular hollow profile problem (dimensions in mm): cross-section geometry (a), three-calibrator layout (b), and one-calibrator layout (c).

Table 2. General Conditions Used in the Simulations.

k_p	0.18 W/mK
k_c	14.0 W/mK
ρ_p	1400 kg/m^3
c_p	1000 J/kgK
Linear extrusion velocity	2 m/min
Profile thickness	3 mm
Cooling channels' diameter	8 mm
Melt inlet temperature	180°C
Room temperature	20°C
Cooling fluid temperature	18°C
Profile/air convection heat transfer coefficient (free convection)	5 W/m^{2}K
Polymer emissivity ε_p	0.9
Calibrator emissivity ε_c	0.25
Profile/calibrator convection heat transfer coefficient (contact resistance)	500 W/m^{2}K
Inner profile boundary	Insulated
CD	12 mm

cooling channels, the type of outer boundary has a negligible impact upon the total loss. However, the usual procedure of considering only convection is inadequate. Anyway, if detailed knowledge of temperature along the extrudate is required, then it is important to consider both the effects of convection and radiation in the annealing zones.

The above computations ignored the contribution of radiation heat exchange between the profile and the transversal external surfaces of the calibrator, as this would make the calculation algorithm much more complex. However, since only a minor part of the heat emitted by radiation by the profile would reach those calibrator surfaces, owing to the low view factors, this omission is irrelevant.

Finally, it is worth noting that a 50% change of h_i, which lies within the practical range of variation, yields

Table 3. Case Studies Considered to Study the Influence of the Boundary Conditions.

Code	Boundary for Outer Surface of Profile + Calibrator	Calibrator/Profile Interface [W/m^{2}K]
$c1r1$	convection + radiation	$h_i = 500$
$c0r0$	adiabatic	$h_i = 500$
$c1r0$	convection	$h_i = 500$
$c0r1$	radiation	$h_i = 500$
$h\uparrow$ (+50%)	convection + radiation	$h_i = 750$
$h\downarrow$ (−50%)	convection + radiation	$h_i = 250$
pc	convection + radiation	Perfect contact

a lower than 10% change in $\bar{T}$ of the extrudate at the end of the cooling zone, in agreement with the variations in the total heat loss. Clearly, this parameter is the major factor affecting the thermal performance of the production line.

Process and Geometrical Parameters

To assess the influence of process and geometrical parameters on cooling, the conditions specified in *Table 2* and the layout shown in *Fig. 12c* (i.e., single 600-mm-long calibrator) were considered. *Table 6* presents a number of case studies, investigating changes in the conditions of *Table 2*, which will be taken as the reference case (ref) for comparison of the results. *Figure 13* illustrates the changes in the layout of the cooling channels, and the corresponding results are listed in *Table 7*.

The effect of the cooling fluid temperature (tw) is much smaller than that of the profile velocity (vp). Additionally, the effect of tw with respect to $\bar{T}$ and σ_T is conflicting, i.e., values that promote a lower $\bar{T}$ will induce higher σ_T and vice versa, as a consequence of the high Biot number ($h\delta/k$) that characterizes heat transfer in plastics, i.e., heat conduction in the bulk is much slower than convection at the interface. Conversely, vp promotes the simultaneous increase or decrease of both $\bar{T}$ and σ_T, which is advantageous for optimization purposes. However, a better cooling performance (which requires low values of $\bar{T}$ and σ_T) involves, not surprisingly, the decrease of vp, i.e., of the production rate.

In the case of geometrical parameters, the use of a zigzag arrangement for the cooling channels (lc, ld), or the increase of the number of cooling channels (lb), favors the decline of T_{min}, T_{max} and $\bar{T}$, but again increase σ_T. The improvements obtained by narrowing a zigzag arrangement (lc) are negligible compared with the use of a wider one (ld). In practice, these marginal advantages will eventually be offset by the higher machining costs, i.e., simpler channels are the best choice for the present case study.

The distance between the cooling channel and the profile surface (cd) is relatively unimportant; its reduction ($cd\downarrow$) has almost no effect on the results, while its increase ($cd\uparrow$) reduces the cooling efficiency. This indicates a limiting cd value below which the increase in cooling efficiency in negligible.

Splitting the calibrator into several smaller units with the same total length (nc) promoted variations of $\bar{T}$ and σ_T with the same sign and is advantageous in relation to the reference case. This is a consequence of the reduction of the heat flux at the polymer surface occurring between two consecutive calibrators, which increases both the temperature homogeneity and the effectiveness of the subsequent cooling, given the increase of the profile surface temperature. Therefore, splitting the calibrator has a thermal effect similar to that of reducing

Table 4. Boundary Heat Fluxes [W] Computed for the Case Studies Listed in Table 3.

Code	Os1	Calibrator I		Os2	Calibrator II		Os3	Calibrator III		Os4	Total
		Calibrator Surface	Cooling Channels		Calibrator Surface	Cooling Channels		Calibrator Surface	Cooling Channels		
$c1r1$	–32.0	–1076.1		–20.7	–736.3		–15.0	–589.8		–7.5	–2477.3
		–15.9	–1060.2		–10.2	–726.1		–7.8	–581.9		
$c0r0$	0.0	–1089.0		0.0	–748.8		0.0	–601.1		0.0	–2438.9
		0.0	–1089.0		0.0	–748.8		0.0	–601.1		
$c1r0$	–10.3	–1085.9		–8.3	–744.4		–6.3	–596.7		–3.3	–2455.3
		–12.3	–1073.6		–8.0	–736.4		–6.2	–590.6		
$c0r1$	–22.3	–1079.0		–12.9	–740.5		–9.0	–593.9		–4.3	–2461.8
		–4.0	–1075.0		–2.5	–738.0		–1.9	–592.0		
$h\uparrow$	–32.0	–1172.7		–18.9	–773.0		–13.5	–609.3		–6.5	–2626.0
		–17.5	–1155.2		–10.8	–762.1		–8.1	–601.1		
$h\downarrow$	–32.0	–859.9		–24.9	–638.0		–19.0	–530.9		–9.9	–2114.4
		–12.3	–847.5		–8.6	–629.3		–6.9	–524.0		
pc	–32.1	–1421.7		–14.9	–848.0		–10.1	–643.8		–4.6	–2975.2
		–21.9	–1399.8		–12.1	–835.9		–8.8	–635.0		

Table 5. Results Computed at the End Cross Section of the Extrudate for the Case Studies of Table 3 (V-Value, D-Relative Difference to Reference Problem *c*1*r*1).

Code		T_{min}	T_{max}	$\bar{T}$	σ_T
*c*1*r*1	V	48.9	136.1	107.9	21.0
	D	—	—	—	—
*c*0*r*0	V	51.2	137.0	109.0	20.8
	D	4.7%	0.7%	1.0%	–1.3%
*c*1*r*0	V	50.1	136.6	108.6	20.9
	D	2.4%	0.4%	0.6%	–0.6%
*c*0*r*1	V	50.0	136.5	108.4	20.9
	D	2.2%	0.3%	0.4%	–0.6%
h↑ (+50%)	V	57.9	143.3	118.5	19.1
	D	–6.1%	–2.3%	–4.0%	3.2%
h↓ (−50%)	V	45.9	133.0	103.6	21.7
	D	18.4%	5.3%	9.8%	–9.3%
pc	V	40.2	125.4	93.4	22.9
	D	–17.9%	–7.8%	–13.4%	8.9%

Table 6. Case Studies Considered To Study the Influence of Process and Geometrical Parameters.

	Code	Parameter	Description
Process Parameters	*tw*↓ *tw*↑	Cooling fluid temperature	T_w = 12°C T_w = 24°C
	vp↓ *vp*↑	Profile velocity	v_p = 1 m/min v_p = 3 m/min
Geometrical Parameters	*nc*	Number of calibrators	The total cooling length is divided by three individual calibrators (*Fig. 12b*)
	la	Cooling channel layout	Four cooling channels close to the profile's corner (*Fig. 13a*)
	lb		Two cooling channels next to each profile side (*Fig. 13b*)
	lc		Top and bottom cooling channels in a narrow zigzag arrangement (*Fig. 13c*)
	ld		Top and bottom cooling channels in a wide zigzag arrangement (*Fig. 13d*)
	cd↓ *cd*↑	Distance of cooling channel to profile surface (CD in Fig. 12a)	CD = 8 mm CD = 16 mm
	dw↓ *dw*↑	Cooling channel diameter	d = 4 mm d = 12 mm

the extrusion velocity (*vp*↓), but without affecting the production rate. In terms of the values obtained for $\bar{T}$ and "total heat removed," it can be concluded that this option has a performance similar to that of layout *lb*, which employs a double number of cooling channels.

Finally, having the cooling channels close to the profile corners (*la*) reduces T_{min} but increases T_{max}, because the profile corners cool more efficiently than the middle. However, since the former were already cooler than the latter, this option does not promote any improvement (in fact, it reduced the total heat removed from the system). This can also be seen in *Fig. 14*, where the predicted downstream profile temperature distribution is plotted both for the reference (*ref*) and *la* case studies.

CONCLUSIONS

A 3D FVM code developed to model the cooling stage of an extrusion line was presented and validated prior to being used for investigating the effect of various process and geometrical parameters on the efficiency of calibration/cooling units. The code is able to handle accurately various practical situations such as the presence of several individual cooling units and the existence of a thermal resistance between the plastic profile and the cooling medium.

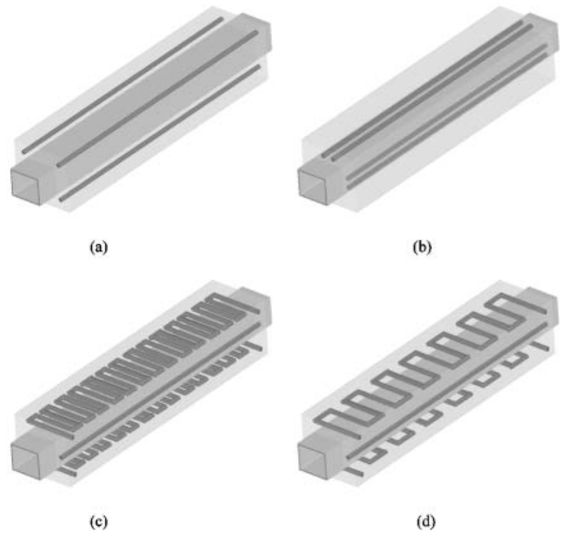

Fig. 13. Variations of the layout of the cooling system (see Table 6): cooling channels close to the profile's corners 'la' (a), two cooling channels close to each profile side 'lb' (b), narrow pitch zigzag arrangement 'lc' (c), and wide pitch zig-zag arrangement 'ld' (d).

Detailed investigation of the calibration unit has shown that most of the heat is removed at the calibrator via the cooling channels and that the contact resistance at the interface is the most important parameter affecting the performance of the unit. Additionally, it was shown that boundary conditions on the calibrator/extrudate outer surfaces have negligible impact.

The effect of process and geometrical parameters on the cooling performance can be quite distinct. Often, when a reduction of the profile average temperature is imparted, lower temperature homogeneity is also obtained, but exceptions are variations in the extrusion velocity and splitting the calibrator into several units. Since the extrudates are characterized by high Biot numbers, significant increases in the heat transfer removal at the extrudate surface quickly reach a limiting behavior (in terms of efficiency), and this should be taken into consideration when designing calibration/cooling units. For instance, the benefits of adopting zigzag cooling channels are clearly insufficient to overcome the increase in machining costs. The effect of other geometrical parameters was not very important, but this may be related to the characteristics of the profile considered.

Table 7. Results Computed at the End Cross Section of the Extrudate and Total Heat Lost for the Case Studies of Table 6 (V-Value, D-Relative Difference to Reference Problem).

	Code		T_{min} [°C]	T_{max} [°C]	$\bar{T}$ [°C]	σ_T [°C]	Total Heat Removed [W]
	ref	**V**	**48.7**	**142.9**	**111.9**	**23.3**	**2340.5**
Process Parameters	*tw*↓	V	44.3	141.6	109.5	24.1	2424.6
		D	–9.1%	–0.9%	–2.2%	3.5%	3.6%
	tw↑	V	53.1	144.2	114.4	22.5	2256.4
		D	9.1%	0.9%	2.2%	–3.5%	–3.6%
	vp↓	V	38.9	99.0	79.1	13.4	1787.0
		D	–20.1%	–30.7%	–29.3%	–42.4%	–23.6%
	vp↑	V	55.3	161.9	128.2	27.2	2697.8
		D	13.4%	13.3%	14.6%	16.9%	15.3%
Geometrical Parameters	*nc*	V	48.9	136.1	107.9	21.0	2477.3
		D	0.4%	–4.8%	–3.6%	–9.6%	5.8%
	la	V	44.4	146.7	116.0	23.0	2200.9
		D	–8.8%	2.6%	3.6%	–1.3%	–6.0%
	lb	V	41.4	139.3	107.9	24.2	2478.9
		D	–15.1%	–2.5%	–3.6%	3.9%	5.9%
	lc	V	32.4	137.4	104.2	25.5	2606.8
		D	–33.6%	–3.8%	–6.9%	9.5%	11.4%
	ld	V	33.6	137.7	105.3	25.3	2567.6
		D	–31.1%	–3.6%	–5.9%	8.6%	9.7%
	cd↓	V	48.7	142.8	110.9	23.5	2373.6
		D	–0.1%	–0.1%	–0.9%	0.9%	1.4%
	cd↑	V	50.1	143.5	113.5	22.9	2286.3
		D	2.8%	0.4%	1.4%	–1.5%	–2.3%
	dw↓	V	52.3	144.4	114.2	22.7	2261.0
		D	7.3%	1.0%	2.1%	–2.3%	–3.4%
	dw↑	V	46.1	141.6	110.0	23.7	2407.5
		D	–5.5%	–0.9%	–1.7%	1.8%	2.9%

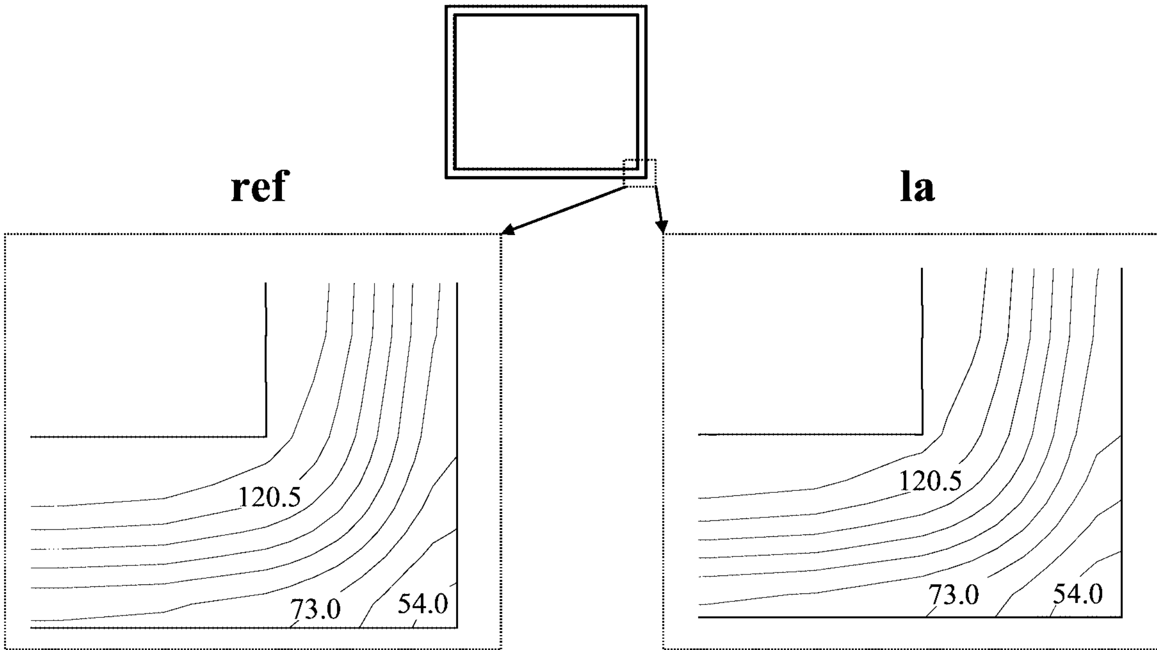

Fig. 14. Temperature fields of the lower-right corner of extrudate cross section downstream, for the reference (ref) and for layout a (la) case studies (Table 6, Temperature in °C).

Given the availability of this modeling tool, which is easily modified to investigate a wide range of processing and geometrical conditions and is relatively fast from a computational point of view, the next stage of development will be its integration into an algorithm for the automatic design of cooling units.

ACKNOWLEDGMENTS

The authors gratefully acknowledge funding by FEDER via FCT, Fundação para a Ciência e Tecnologia, under the POCTI and Plurianual programmes.

REFERENCES

1. V. Kleindienst, *Kunststoffe*, **63(1)**, 7 (1973).
2. W. Michaeli, E*xtrusion Dies for Plastics and Rubber: Design and Engineering Computations*, 2nd Ed., Hanser Publishers, Munich, Vienna, New York (1992).
3. L. Fradette, P. A. Tanguy, F. Thibault, P. Sheehy, D. Blouin, and P. Hurez, *J. Polymer Engineering*, **14(4)**, 295 (1995).
4. R. J. Brown, *SPE ANTEC Tech Papers*, **46**, 383 (2000).
5. B. Endrass, *Kunststoffe-German Plastics*, **83(8)**, 584 (1993).
6. H. O. Schiedrum, *Kunststoffe-German Plastics*, **73(1)**, 2 (1983).
7. H. D. Kurz, *Kunststoffe-German Plastics*, **78(11)**, 1052 (1988).
8. J. F. T. Pittman, G. P. Whitham, S. Beech, and D. Gwynn, *International Polymer Processing*, **9(2)**, 130 (1994).
9. P. Sheehy, P. A. Tanguy, and D. Blouin, *Polym. Eng. Sci.*, **34**, 650 (1994).
10. L. Placek, J. Svabik, and J. Vlcek, *SPE ANTEC Tech. Papers*, **46**, 378 (2000).
11. I. Szarvasy and R. Sander, *Kunststoffe-Plast Europe*, **89(6)**, 7 (1999).
12. A. Gaspar-Cunha and J.A. Covas, *International Polymer Processing*, **16(3)**, 229 (2001).
13. O. S. Carneiro, J. M. Nóbrega, F. T. Pinho, and P. J. Oliveira, “Automatic Design of Profile Extrusion Dies: Experimental Assessment,” in *The Polymer Processing Society, Europe/Africa Regional Meeting*, Athens (2003).
14. J. Vlachopoulos, “Recent Progress and Future Challenges in Computer-Aided Polymer Processing Analysis and Design,” in *ATV-Semapp Meeting*, Funen, Odense, Denmark (1998).
15. W. Dietz, *Polym. Eng. Sci.*, **18**, 1030 (1978).
16. G. Menges, E. Haberstroh, and W. Janke, *Kunststoffe-German Plastics*, **72(6)**, 332 (1982).
17. G. Menges, M. Kalwa, and J. Schmidt, *Kunststoffe-German Plastics*, **77(8)**, 797 (1987).
18. I. Szarvasy, “Simulation of Complex PVC Window Profile Cooling During Calibration with Particular Focus on Internal Heat Exchange,” in *3rd ESAFORM Conference on Material Forming*, Stuttgart, Germany (2000).
19. J. F. T. Pittman and I. A. Farah, *Plastics, Rubber and Composites Processing and Applications*, **25(6)**, 305 (1996).
20. L. Fradette, P. A. Tanguy, P. Hurez, and D. Blouin, *International J. Numerical Methods for Heat & Fluid Flow*, **6(1)**, 3 (1996).
21. J. F. T. Pittman, I. A. Farah, D. H. Isaac, and A. Eccott, “Transfer Coefficients in Spray Cooling of Plastic Pipes,” in *Plastics Pipes IX*, Edinburgh, U.K. (1995).
22. J. M. Nóbrega, F. T. Pinho, P. J. Oliveira, and O. S. Carneiro, *International J. Heat and Mass Transfer*, **47**, 1141 (2004).
23. P. J. Oliveira and F. T. Pinho, *Numerical Heat Transfer Part B-Fundamentals*, **35(3)**, 295 (1999).
24. P. J. Oliveira, F. T. Pinho, and G. A. Pinto, *J. Non-Newtonian Fluid Mechanics*, **79(1)**, 1 (1998).
25. J. H. Ferziger and M. Peric, *Computational Methods for Fluid Dynamics*, Springer Pub. (1999).
26. W. Obendrauf, G. R. Langecker, and W. Friesenbichler, *International Polymer Processing*, **13(1)**, 71 (1998).
27. J. F. T. Pittman, G. P. Whitham, and I. A. Farah, *Polym. Eng. Sci.*, **35**, 921 (1995).
28. Polyflow, Fluent Inc. (http://www.fluent.com).
29. J.M. Nóbrega, *Computer Aided Design of Forming Tools for the Production of Thermoplastic Profiles*, PhD Thesis, Department of Polymer Engineering, University of Minho, Guimarães, Portugal (2004).